

LAND USE AND LAND COVER MAPPING FOR THE MEKONG RIVER DELTA REGION USING LANDSAT-8 SATELLITE IMAGES

Nguyen Huy Trung*, Hoang Huu Chien, Nguyen Quang Thi, Nguyen Duy Hai, Duong Minh Ngoc, Nguyen Ngoc Anh, Vu Thi Hoa

TNU - University of Agriculture and Forestry

ARTICLE INFO	ABSTRACT
<p>Received: 19/10/2022</p> <p>Revised: 14/4/2023</p> <p>Published: 19/4/2023</p>	<p>Land-use/land-cover maps provide fundamental information to support management activities of natural resources and environmental problems. Landsat-8 satellite provides valuable spectral data for deriving accurate regional land-use/land-cover maps. This study demonstrated an approach for mapping land-use/land-cover by combining Landsat-8 images with a high-quality reference dataset in a classification model using the Support Vector Machine algorithm. A spatial explicit land-use/land-cover map at a spatial resolution of 30 m was created for Vietnam's Mekong River Delta (approximately 4.0 million ha). The resulted map obtained an overall accuracy of 80.7%. Though paddy rice is the dominant land-use/land-cover type (covering nearly 1.9 million ha), aquaculture farms (including rice/mangroves-aquaculture) cover a large part of the region (about 784.4 thousand ha). Results from this study provide decision-makers with a comprehensive picture of current land-use/land-cover and facilitate better adjustments to future development plans in the Mekong River Delta. The mapping methods used in this study can be replicated in other regions.</p>
<p>KEYWORDS</p> <p>Land-use map</p> <p>Land-cover map</p> <p>Landsat-8 image</p> <p>Mekong River Delta</p> <p>Bio-aquaculture</p>	

THÀNH LẬP BẢN ĐỒ SỬ DỤNG ĐẤT/LỚP PHỦ BỀ MẶT TẠI VÙNG ĐỒNG BẰNG SÔNG CỬU LONG SỬ DỤNG ẢNH VỆ TINH LANDSAT-8

Nguyễn Huy Trung*, Hoàng Hữu Chiến, Nguyễn Quang Thi, Nguyễn Duy Hải, Dương Minh Ngọc, Nguyễn Ngọc Anh, Vũ Thị Hòa

Trường Đại học Nông lâm – ĐH Thái Nguyên

THÔNG TIN BÀI BÁO	TÓM TẮT
<p>Ngày nhận bài: 19/10/2022</p> <p>Ngày hoàn thiện: 14/4/2023</p> <p>Ngày đăng: 19/4/2023</p>	<p>Bản đồ sử dụng đất/lớp phủ bề mặt cung cấp các thông tin quan trọng hỗ trợ công tác quản lý tài nguyên thiên nhiên và môi trường. Vệ tinh Landsat-8 cung cấp dữ liệu ảnh đa phổ có giá trị để thành lập bản đồ sử dụng đất/lớp phủ bề mặt với độ chính xác cao. Nghiên cứu này xây dựng một phương pháp thành lập bản đồ dụng đất/lớp phủ bề mặt bằng cách kết hợp dữ liệu ảnh Landsat-8 với dữ liệu tham khảo chất lượng cao trong một mô hình phân loại sử dụng thuật toán Máy Vector Hỗ trợ. Bản đồ sử dụng đất/lớp phủ bề mặt năm 2021 được thành lập cho toàn bộ vùng Đồng bằng sông Cửu Long (tổng diện tích khoảng 4 triệu ha) với độ phân giải không gian 30 m. Bản đồ kết quả có độ chính xác tổng thể khoảng 80,7%. Mặc dù lúa nước là loại hình sử dụng đất chính (chiếm 1,9 triệu ha), đất sử dụng để nuôi trồng thủy sản (bao gồm cả các mô hình kết hợp lúa hoặc rừng ngập mặn với thủy sản) cũng chiếm một phần lớn diện tích toàn vùng (khoảng 784,4 nghìn ha). Kết quả từ nghiên cứu này cung cấp cho các nhà hoạch định một bức tranh toàn cảnh về hiện trạng sử dụng đất/che phủ bề mặt, hỗ trợ điều chỉnh và lập quy hoạch phát triển ở Đồng bằng sông Cửu Long trong tương lai. Các phương pháp sử dụng trong nghiên cứu này có tính khả thi để áp dụng ở các vùng khác.</p>
<p>TỪ KHÓA</p> <p>Bản đồ sử dụng đất</p> <p>Bản đồ lớp phủ bề mặt</p> <p>Ảnh Landsat-8</p> <p>Đồng bằng sông Cửu Long</p> <p>Mô hình thủy sản sinh thái</p>	

DOI: <https://doi.org/10.34238/tnu-jst.6720>

* Corresponding author. Email: nguyenhuytrung@tuaf.edu.vn

1. Introduction

Land-use is the term referring to the functional use of land by humans while land-cover is the term referring to the physical material of the Earth's surface. Land-use/land-cover (LULC) maps are important to explain complex relationships between humans and the environment [1]. They provide fundamental information to support the implementation of policies related to the management of natural resources and environmental problems such as deforestation, climate change, natural hazards and agricultural practices [2]. Therefore, it has always been of great interest to geospatial science and remote sensing communities to produce more accurate and up-to-date LULC maps, especially at regional scales.

River delta often experiences the most significant LULC changes due to the high concentration of population and the impact of climate change. The Mekong River Delta (MRD), known as the world's third-largest delta, is globally recognized as an important agricultural production region and biodiversity hotspot. Over recent decades, LULC in the Mekong Delta has experienced tremendous changes due to both increasing natural and anthropogenic activities [1], [2]. Hence, it is necessary to create accurate LULC mapping products for the entire delta region that support better LULC monitoring and planning activities across the region.

The use of remote sensing satellite data became popular in the 1980s with the increasing and consistent availability of satellite images to the public. LULC studies usually applied satellite data with moderate (250 m) to high (5 m) spatial resolution, depending on the detail requirements and available resources [3]. It has been discussed in many studies that low-moderate resolution sensors are not appropriate for high-precision LULC classifications at regional scales [3], [4]. For many applications, information is required at fine spatial resolutions and medium-resolution sensors (10-30 m), such as Landsat and Sentinel as they are more adequate to detect most human-environment interactions [3]. Since the opening of Landsat's archive in 2008, the use of Landsat data significantly increased because of the free access to its 40 years of earth observation data. Many countries have generated regional and nationwide LULC maps primarily based on Landsat data [5], [6]. Among Landsat missions, Landsat-8, launched in 2013, provides valuable spectral data to improve the quality of LULC mapping. It carries two sensors that are Operational Land Imager (OLI) and Thermal InfraRed Sensor (TIRS), with a temporal resolution of 16 days. Landsat-8 OLI images provide five visible and near-infrared (NIR) bands and two short-wave infrared (SWIR) bands processed to orthorectified surface reflectance, and two thermal infrared (TIR) bands processed to orthorectified brightness temperature. Spectral bands are often combined with vegetation indices, such as Normalized Difference Vegetation Index (NDVI) and Enhanced Vegetation Index (EVI), to provide accurate LULC classification results [7], [8].

Many classification techniques can be applied for LULC mapping from Landsat satellite images. Machine learning methods commonly used for image classification include Random Forest, Support Vector Machines and K-Nearest Neighbour [9]-[11]. However, studies have concluded that the performance of a LULC classification model is more dependent on the quality of the sample dataset than on the classification techniques [3]. Conventionally, high-quality sample data are usually collected from field surveys which are normally costly and time/labour-consuming. Recent studies have proposed human-interpretation methods as a more cost-effective approach to deriving high-quality sample data. In these methods, experienced experts determine the LULC status of a given sample by interpreting other products such as high-resolution Google Earth images and aerial photos if available [12]-[14].

This study aimed to demonstrate an approach for accurate LULC mapping across the MRD region by combining Landsat-8 OLI images with a high-quality reference dataset created using a human-interpretation method. This study provides a cost-effective LULC mapping method that can be replicated in other regions and informs decision-makers and managers of a comprehensive understanding of the current LULC in MKD.

2. Materials and Methods

2.1. Study area

The study area was the MRD, also known as the Nine Dragon River Delta, encompassing a large portion of southwestern Vietnam (approximately 4.0 million ha). The region comprises 13 administrative provinces with the province-level municipality of Can Tho (Figure 1). MRD is a relatively flat and low-elevated region, with a mean elevation of ~0.8 m (ranging from 0.3-2 m) above the sea level [15]. The region is dominated by a tropical monsoon climate and characterised by two yearly seasons, including the rainy season from May to November and the dry one from December to April. The annual average temperature is around 27°C and annual precipitation ranges from 1,800 to 2,300 mm, mainly distributed in the rainy season. MRD is highly sensitive and vulnerable to climate change [16]. MRD is a key agricultural production area of Vietnam. It is the largest rice production area of the country with more than half of the total land area being used for rice production (about 1.8 million ha), supplying approximately 50% of rice for domestic use and about 90% for exporting [17]. In recent years, with great promotion from the Government, aquaculture and fruit plantations have been significantly expanded in MRD, causing major transitions among LULC types [18]. Some sustainable aquaculture farming models, such as rice-shrimp/fish and mangroves-shrimp, have become more common across the region [19].

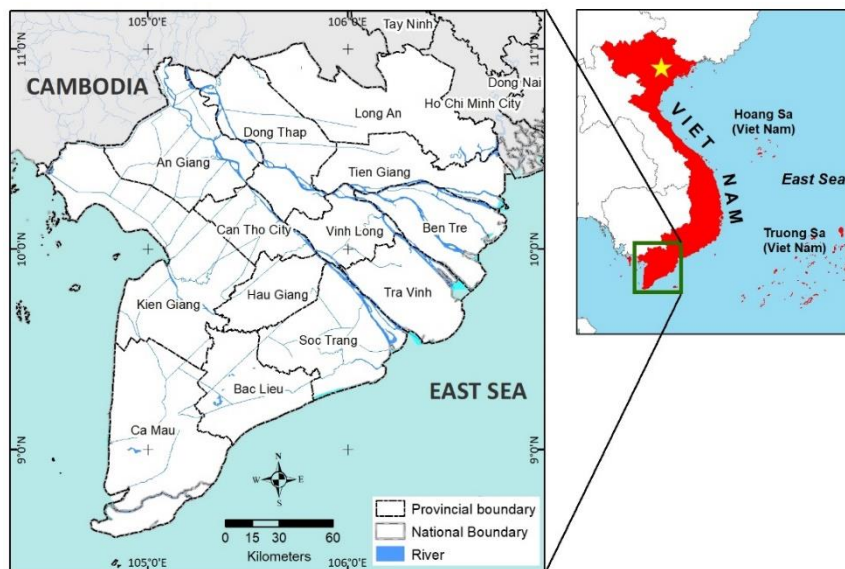


Figure 1. The study area

2.2. Data and pre-processing

2.2.1. Landsat-8 data

Landsat-8 OLI surface reflectance images (Level 2, Collection 2, Tier 1) covering the study area and acquired during 2021 were processed using Google Earth Engine (GEE) platform [20]. These products have a spatial resolution of 30 m. They were atmospherically corrected using the Land Surface Reflectance Code (LaSRC) algorithm and included a cloud/shadow mask produced using the CFMask algorithm, as well as a per-pixel saturation mask [21]. These images contain four visible bands, one NIR band and two SWIR bands processed to orthorectified surface reflectance (Table 1). A cloud-free composite image of all Landsat 8 OLI scenes was created using the best-available-pixel tool integrated into GEE. Vegetation indices including NDVI and EVI then were computed using the Landsat-8 composite (Table 1).

2.2.2. Supplemental data

Road and hydrological systems in MRD are complex with many narrow roads and rivers/streams that are normally difficult to define from satellite data. To overcome this challenge, accurate road and river data layers were derived from Open Street Map (OSM) to complement the final LULC map. These layers were transformed into the raster format aligning with the spatial resolution of Landsat-8 data.

Table 1. Landsat 8 OLI bands and vegetation indices

Band/Index	Wavelength (μm)	Description
Spectral bands		
Band 1	0.43-0.45	Coastal aerosol
Band 2	0.45-0.51	Blue
Band 3	0.53-0.59	Green
Band 4	0.64-0.67	Red
Band 5	0.85-0.88	NIR
Band 6	1.57-1.65	SWIR-1
Band 7	2.11-2.29	SWIR-2
Vegetation indices		
NDVI	$\text{NDVI} = (\text{NIR} - \text{Red}) / (\text{NIR} + \text{Red})$	
EVI	$\text{EVI} = 2.5 * ((\text{NIR} - \text{Red}) / (\text{NIR} + 6 * \text{Red} - 7.5 * \text{Blue} + 1))$	

2.2.3. Reference dataset

A reference dataset consisting of 850 plots was created using a random sampling method. The size of each sample plot was 90 m x 90 m which aligns with a window of 3x3 Landsat pixels. The LULC status of each plot was attributed using a multiple-lines-of-evidence approach, in which experienced remote sensing experts interpreted Google Earth high-resolution images, Landsat-8 images and other supporting data (e.g., previous LULC). From the reference dataset, 12 LULC classes were defined for Mekong Delta as shown in Table 2. The reference dataset was divided into two parts, in which ~70% of sample plots (607 plots) were used as training data classification model development and the remaining ~30% (243 plots) was used for map accuracy assessment. Table 2 shows the number of plots used for training and validation by each LULC type.

Table 2. LULC types identified for MRD and the associated number of sample plots

LULC types	Number of sample plots	
	Training	Validation
Paddy rice	104	42
Upland crops	30	12
Salt farm	38	15
Other agriculture	23	9
Aquaculture	75	30
Bio-Aquaculture (i.e., rice/forest-aquaculture)	53	21
Plantations	63	25
Forests	38	15
Mangroves	43	17
Built-ups	65	26
Water	50	20
Bare ground	28	11
Total	607	243

2.3. Image classification and assessment methods

2.3.1. Image classification model

A LULC classification model was developed using the Maximum Likelihood Classification (MLC) algorithm that is included as a tool in the ArcGIS software package. The MLC algorithm is based on the maximum likelihood probability theory. It assigns each pixel to one of the different classes based on the means and variances of the class signatures (stored in a signature file). Independent variables (predictors) of the model included six Landsat-8 bands (2 to 7) and two computed vegetation indices (NDVI and EVI). Model training data were 607 sample plots extracted from the reference dataset. Training samples were used to identify LULC classes from spectral satellite data based on their specific signature properties. To make sure that the LULC classes represented by the training samples are distinguishable from Landsat remote sensing signals, their spectral characteristics were checked and compared by examining the histograms for each class.

2.3.3. Post-classification processing

In the pixel-based classified LULC map, there could be some misclassifications that produced isolated pixels or small areas of pixels. Therefore, post-classification processing steps were conducted to remove the noise and thus improve the quality of the classified map. In particular, the post-classification processing task involved three steps: (i) filtering the classified map, (ii) smoothing and clumping class boundaries, and (iii) generalizing the map by removing small isolated regions. The task was done by using a set of spatial processing tools provided in the ArcGIS Spatial Analyst extension.

2.3.4. Final map and accuracy assessment

The final LULC map of MRD was produced by merging the Landsat-derived map with supplemental road and river layers. Roads are classified on the map as built-up areas. Map accuracy was assessed using the validation dataset (243 sample plots, Table 2) and represented by a confusion matrix.

3. Results and discussions

3.1. Land use/land cover in the Mekong River Delta

Figure 2 presents the LULC map of 2021 for the MRD region and Table 3 shows the total area and proportion of each LULC type. Overall, agricultural lands cover the major part of the region (over 83% of the total area). Unsurprisingly, paddy rice, the key agriculture form in MRD, is the dominant LULC type, covering nearly 1.9 million ha (47.4% of the total area). Whereas, upland crops (e.g., corn, black sesame, chilli) cover a much smaller area compared with rice, around 152.3 thousand ha (3.88% of total area), distributed mainly in Long An, Tien Giang and Hau Giang provinces. Aquaculture is the second largest agriculture model in the region, following paddy rice. Aquaculture lands are developed along the coastal line from Ben Tre to Ca Mau and account for 17.15% of the total region area (about 672.1 thousand ha). It is the main agriculture form along the coastal areas from Ben Tre to Ca Mau provinces. Bio-aquaculture (i.e., mangroves/rice-aquaculture) is considered a sustainable agriculture model and has been recently expanded in MRD. The mapping result shows that the total area of bio-aquaculture in MRD is approximately 112.4 thousand ha (2.87% of the total area) in 2021, mostly in Ca Mau, Bac Lieu and Soc Trang.

Salt farms are common in Bac Lieu, Ben Tre, and Soc Trang provinces with a total area of about 5.1 thousand ha. The total area of plantations (mainly fruit trees) is approximately 481.5 thousand ha, mainly distributed in Ben Tre, Vinh Long, and Can Tho. The area of forests and mangroves is roughly 81.0 and 9.4 thousand ha, respectively. It is important to note that the actual area of mangroves in MRD is about 73.4 thousand ha but the major part has been used for aquaculture (classified as bio-aquaculture). Water bodies in MRD cover a total area of 212.3 thousand ha and the area of built-ups is about 328.2 thousand ha.

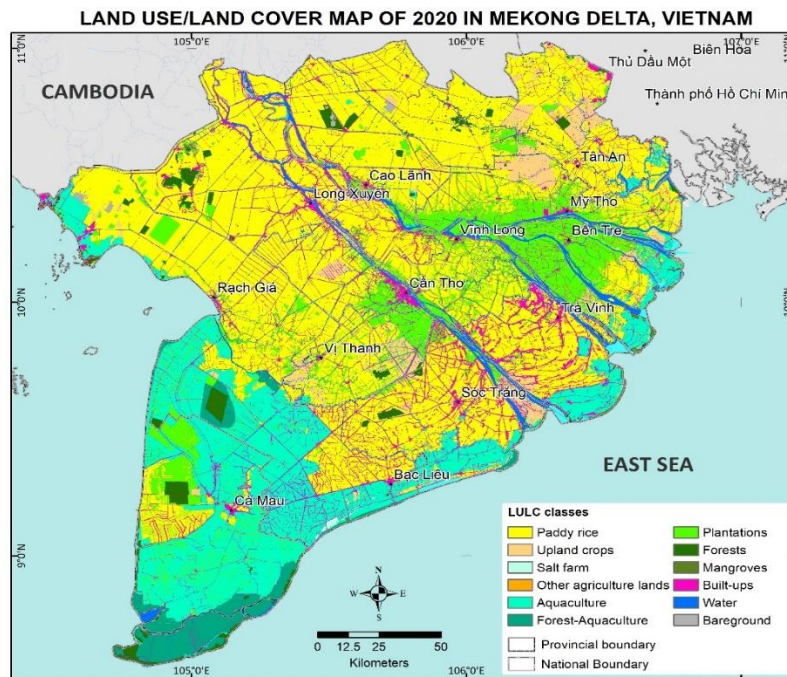


Figure 2. LULC map of 2021 for the MRD region

Table 3. Total area and rate by LULC types in MRD

No.	LULC type	Area	Proportion (%)
1	Paddy rice	1,857,848.9	47.40
2	Upland crops	152,265.9	3.88
3	Salt farm	5,092.9	0.13
4	Other agriculture	391.5	0.01
5	Aquaculture	672,071.3	17.15
6	Bio-Aquaculture	112,393.0	2.87
7	Plantations	481,513.0	12.29
8	Forests	81,009.1	2.07
9	Mangroves	9,391.5	0.24
10	Built-ups	328,188.7	8.37
11	Water	212,287.2	5.42
12	Bare ground	7,007.1	0.18
Total		3,919,460.0	100

3.2. Accuracy assessment

The final LULC map obtained an overall accuracy of 80.7% (Table 4). The paddy rice class, with the largest number of observation samples, achieved the highest user's and producer's accuracies, 85.7% for both. The lowest accuracies were found within salt farms, bare ground and other agriculture classes but not lower than 70.0%. Results from our classification model confirmed that main LULC types in MRD can be identified and mapped reliably by combining Landsat-based metrics (spectral bands and indices) with an extensive reference dataset created using a multiple-lines-of-evidence approach (mainly based on Google Earth high-resolution images). Importantly, the bio-aquaculture class (mangroves/rice-aquaculture) was distinguishable from mangroves and paddy rice given it obtained relatively high producer's and user's accuracies, 81.0% and 77.3%, respectively. Similarly, mangroves were distinguishable from forests and plantations. Confusion, or errors, predominately occurred between similar classes but were not significant (Table 4). For instance, there were often misplacements of observations between

forests and plantations or paddy rice and aquaculture, or built-ups and bare ground. There could be several ways to avoid these common misclassifications and thus improve the accuracy of the LULC. Some recent studies demonstrated that a combination of optical satellite data, such as Landsat-8 and Sentinel-2, and radar satellite data, such as Sentinel-1, can improve the quality of LULC mapping products [22], [23]. This may require further investigations in remote sensing data processing and classification methods which are interesting topics for studies in the future.

Table 4. Confusion matrix of the LULC map

Classified data	Reference data												Total	UA (%)
	PR	UR	SF	OA	AQ	BA	PL	FR	MG	BU	WT	BG		
PR	36	1	1	1	1	1					1		42	85.7
UR	1	9		1								1	12	75.0
SF			11		1					1			13	84.6
OA			2	7						1			10	70.0
AQ	2		1		23						2		28	82.1
BA	1				2	17			2				22	77.3
PL		1					21	2	1				25	84.0
FR							2	12	1				15	80.0
MG						2	2	1	13				18	72.2
BU	1				1					22		2	26	84.6
WT	1				2	1					17		21	81.0
BG		1	0							2		8	11	72.7
Total	42	12	15	9	30	21	25	15	17	26	20	11		Overall accuracy
PA (%)	85.7	75.0	73.3	77.8	76.7	81.0	84.0	80.0	76.5	84.6	85.0	72.7		80.7%

(PR = Paddy rice, UR = Upland crops, SF = Salt farm, OA = Other agriculture, AQ = Aquaculture, BA = Bio-Aquaculture, PL = Plantations, FR = Forests, MG = Mangroves, BU = Built-ups, WT = Water, BG = Bareground; PA = Producer's Accuracy, UA = User's accuracy)

4. Conclusion

This study investigated the distribution of key LULC types in the MRD region at a spatial resolution of 30 m. Overall, the mapping results indicated that reliable LULC maps at regional scales can be derived by using Landsat-8 OLI images in combination with a high-quality reference dataset created using a human-interpretation method. The 2021 LULC map of MRD obtained an overall accuracy of 80.7%. Some integrated aquaculture models, such as bio-aquaculture, were quantified with relatively high accuracies. Though paddy rice was the dominant LULC type, covering nearly 1.9 million ha (47.4% of the total area), aquaculture farms (including bio-aquaculture) covered a large part of the region (accounting for approximately 20% of the total area). Results from this study provide decision makers with a comprehensive picture of current LULC in MRD and facilitate better adjustments to future land use plans.

REFERENCES

- [1] T. N. Le, A. K. Bregt, G. E. van Halsema, P. J. Hellegers, and L.-D. Nguyen, "Interplay between land-use dynamics and changes in hydrological regime in the Vietnamese Mekong Delta," *Land use policy*, vol. 73, pp. 269-280, 2018.
- [2] S. CCAFS, *Assessment Report: The drought and salinity intrusion in the Mekong River Delta of Vietnam*, ed: Hanoi, 2016.
- [3] M. E. D. Chaves, M. C. A. Picoli, and I. D. Sanches, "Recent Applications of Landsat 8/OLI and Sentinel-2/MSI for Land Use and Land Cover Mapping: A Systematic Review," *Remote Sensing*, vol. 12, no. 18, 2020, doi: 10.3390/rs12183062.
- [4] L. Yu, J. Su, C. Li, L. Wang, Z. Luo, and B. Yan, "Improvement of Moderate Resolution Land Use and Land Cover Classification by Introducing Adjacent Region Features," *Remote Sensing*, vol. 10, no. 3, 2018, Art. no. 414.

- [5] S. Chowdhury, D. K. Chao, T. C. Shipman, and M. A. Wulder, "Utilization of Landsat data to quantify land-use and land-cover changes related to oil and gas activities in West-Central Alberta from 2005 to 2013," *GIScience & Remote Sensing*, vol. 54, no. 5, pp. 700-720, 2017.
- [6] C. Homer *et al.*, "Completion of the 2011 National Land Cover Database for the conterminous United States—representing a decade of land cover change information," *Photogrammetric Engineering & Remote Sensing*, vol. 81, no. 5, pp. 345-354, 2015.
- [7] M. L. Clark, "Comparison of multi-seasonal Landsat 8, Sentinel-2 and hyperspectral images for mapping forest alliances in Northern California," *ISPRS Journal of Photogrammetry and Remote Sensing*, vol. 159, pp. 26-40, 2020.
- [8] P. Teluguntla *et al.*, "A 30-m landsat-derived cropland extent product of Australia and China using random forest machine learning algorithm on Google Earth Engine cloud computing platform," *ISPRS Journal of Photogrammetry and Remote Sensing*, vol. 144, pp. 325-340, 2018.
- [9] H. T. T. Nguyen, T. M. Doan, and V. Radeloff, "Applying random forest classification to map land use/land cover using Landsat 8 OLI," *The International Archives of the Photogrammetry, Remote Sensing and Spatial Information Sciences*, vol. 42, no. 3, p. W4, 2018.
- [10] H. T. T. Nguyen, T. M. Doan, and V. Radeloff, "Applying Random Forest Classification to Map Land Use/Land Cover Using Landsat 8 Oli," *The International Archives of the Photogrammetry, Remote Sensing and Spatial Information Sciences*, vol. XLII-3/W4, pp. 363-367, 2018, doi: 10.5194/isprs-archives-XLII-3-W4-363-2018.
- [11] C. Liping, S. Yujun, and S. Saeed, "Monitoring and predicting land use and land cover changes using remote sensing and GIS techniques—A case study of a hilly area, Jiangle, China," *PloS one*, vol. 13, no. 7, 2018, Art. no. e0200493.
- [12] J. Chen *et al.*, "Global land cover mapping at 30 m resolution: A POK-based operational approach," *ISPRS Journal of Photogrammetry and Remote Sensing*, vol. 103, pp. 7-27, 2015.
- [13] C. W. Rathnayake, S. Jones, and M. Soto-Berelov, "Mapping land cover change over a 25-year period (1993–2018) in Sri Lanka using Landsat time-series," *Land*, vol. 9, no. 1, p. 27, 2020.
- [14] M. Soto-Berelov, A. Haywood, S. Jones, S. Hislop, and T. H. Nguyen, "Creating a Robust Reference Dataset for Large Area Time Series Disturbance Classification," in *Remote Sensing Time Series Image Processing*, CRC Press, 2018, pp. 157-171.
- [15] P. S. J. Minderhoud, L. Coumou, G. Erkens, H. Middelkoop, and E. Stouthamer, "Mekong delta much lower than previously assumed in sea-level rise impact assessments," *Nat Commun*, vol. 10, no. 1, p. 3847, Aug. 28, 2019, doi: 10.1038/s41467-019-11602-1.
- [16] B. T. Yen, N. H. Son, L. T. Tung, T. S. Amjath-Babu, and L. Sebastian, "Development of a participatory approach for mapping climate risks and adaptive interventions (CS-MAP) in Vietnam's Mekong River Delta," *Climate Risk Management*, vol. 24, pp. 59-70, 2019, doi: 10.1016/j.crm.2019.04.004.
- [17] R. Cramb, *White gold: The commercialisation of rice farming in the lower Mekong Basin*. Springer Nature, 2020.
- [18] Q. H. Nguyen *et al.*, "Land-use dynamics in the Mekong delta: From national policy to livelihood sustainability," *Sustainable development*, vol. 28, no. 3, pp. 448-467, 2020.
- [19] H. D. Dang, "Sustainability of the rice-shrimp farming system in Mekong Delta, Vietnam: a climate adaptive model," *Journal of Economics and Development*, vol.22, pp.21-45, 2020.
- [20] USGS, "USGS Landsat 8 Level 2, Collection 2, Tier 1," 2021. [Online]. Available: https://developers.google.com/earth-engine/datasets/catalog/LANDSAT_LC08_C02_T1_L2. [Accessed date 15 April 2022].
- [21] S. Foga *et al.*, "Cloud detection algorithm comparison and validation for operational Landsat data products," *Remote sensing of environment*, vol. 194, pp. 379-390, 2017.
- [22] I. Dino *et al.*, "Combining Sentinel-1 and Sentinel-2 Satellite Image Time Series for land cover mapping via a multi-source deep learning architecture," *ISPRS Journal of Photogrammetry and Remote Sensing*, vol. 158, pp. 11-22, 2019.
- [23] T. T. H. Nguyen *et al.*, "Mapping Land use/land cover using a combination of Radar Sentinel-1A and Sentinel-2A optical images," *IOP Conference Series: Earth and Environmental Science*, vol. 652, no. 1, IOP Publishing, 2021.